Mathematical modelling of uniaxial extension of a heterogeneous gas cell wall in bread dough: Stress fields and stress concentration analysis relating to the proving and baking steps

Kossigan Bernard Dedey, David Grenier, Tiphaine Lucas

Mathematical modelling of uniaxial extension of a heterogeneous gas cell wall in bread dough: stress fields and stress concentration analysis relating to the proving and baking steps

Author names and affiliations

Kossigan Bernard DEDEY [1,2], David GRENIER [2*], Tiphaine LUCAS [2]

[1]Université Rennes 1, avenue du Général Leclerc, 35042 Rennes Cedex, France

[2]INRAE, UR OPAALE, F-35044 Rennes, France

kossigan.dedey@inrae.fr, david.grenier@inrae.fr* and tiphaine.lucas@inrae.fr

***Corresponding author**

INRAE, UR OPAALE, 17 avenue de Cucillé, F-35044 Rennes Cedex, France

Abstract

A mathematical model was developed to increase the understanding of stress concentrations within a gas cell wall (GCW) in bread dough during baking. The GCW was composed of a single A-type wheat starch granule surrounded by various proportions of gluten typical of GCWs when about to rupture. Finite element simulations were carried out in 2D using linear viscoelasticity and visco-hyperelasticity. Strain orders of magnitude and rates relevant to dough during baking were applied as boundary conditions for two plausible sets of mechanical properties before and after protein coagulation and starch gelatinization (T < 50-60°C and T > 70-80°C). The average stress within the GCW was found to be strongly dependent on the starch fraction. Gluten-starch interactions influenced average stress values considerably when the starch fraction was greater than 11% v/v. The locations within the GCW where rupture was most likely to be initiated were identified by mapping maximal stress points using stress field and triaxiality analysis and the findings were discussed.

Keywords: viscoelasticity, visco-hyperelasticity, rupture

1 Introduction

Bread dough can be viewed as a dispersion of gas cells in a continuous hydrated gluten-starch matrix (Gan et al., 1990). The crumb structure of baked breads (specific volume, gas fraction and texture) mostly depends on dough preparation before baking i.e. mixing and proving (Dobraszczyk, 2017; Eliasson and Larsson, 1993) but also, to a great extent, on the way the walls that separate the gas cells (GCWs) rupture during baking (Dobraszczyk, 2017; Hayman et al., 1998). When early GCW rupture occurs i.e. below both gelatinization and protein coagulation temperatures, the crumb collapses and large cells form within it. When the opposite occurs, and only a few or none of the GCWs rupture during baking, there is shrinkage at the cooling stage that follows due to the decrease in pressure in the cells that have remained closed (Kusunose et al., 1999). At the end of fermentation and during baking, some of the thinnest GCWs are reduced to approximately the size of starch granules (Bloksma, 1990; Sandstedt, 1954). These are the GCWs most likely to rupture. When such a size is reached, gluten and starch granules must be considered as interacting phases to account for their structural heterogeneities. The individual mechanical properties of phases and the interactions between them are crucial to any proper description of stress concentrations and of the areas where rupture is most likely to be initiated within GCWs.

The mechanical properties of composite materials such as GCWs in bread dough result from the collective mechanical properties of the separate constituents present in dough and from the interactions between them. In bread dough the chief constituents are starch, gluten and water. Numerous studies have been devoted to the characterization of the individual mechanical properties of gluten (Dreese et al., 1988; Faubion et al., 1985; Janssen et al., 1996; Kokelaar et al., 1996; Ng, 2007; Wesołowska-Trojanowska et al., 2014) and of starch granules (Chiotelli and Le Meste, 2002; Herrera et al., 2017). Studies have been performed at temperatures higher than 25°C on dough or gluten but these are generally carried out using dynamic tests (Dreese et al., 1988). The applied strain and strain rates (> 10^{-2} s^{-1}) in these studies were greater than those that occur during GCW extension in the course of baking, where strain rates are of the order of 10^{-3} s^{-1} (Lucas et al., 2020). The conditions for most methods are such that the link between rheology and baking performance is not a straightforward one (Dobraszczyk, 2017). During baking, half of the initial extensibility of the gluten is lost at about 65°C and a proportion of the other half by the end of baking (90°C) (Attenburrow et al., 1990; Grenier et al., 2021). In the case of starch alone, studies at temperatures above 25°C have been carried out in excess water (Carrington et al., 1998;

Desse et al., 2010; Fisher et al., 1997). At 25°C starch granules are non-deformable at pressures of the order of magnitude found in bread baking. When heated at 65°C in excess water, starch granules soften and become easily deformable (strain > 1.4) under shearing and compression. The behaviour of starch is strongly dependent on water content and the mechanical properties identified in excess water have little or no application to starch at water contents relevant to bread dough during baking. To the best of our knowledge, no work exists that addresses the mechanical properties of starch and gluten separately in controlled hydrothermal conditions relevant to those affecting GCWs during bread dough baking. For this reason, it is hard to obtain the mechanical parameters relevant to the full temperature range encountered during bread dough baking (25-140°C). Only the orders of magnitude of these mechanical properties can be captured. Mohammed et al. (2013) identified values for starch and gluten using Young's moduli of 90 kPa and 10 kPa respectively (with relaxation times of 100 s for starch and 10 s for gluten) for bread dough at room temperature and demonstrated that there was close agreement between numerical simulations and the experimental data. This makes it possible to rely on the orders of magnitude of the moduli selected for the present study.

Various constitutive models have been used to describe the mechanical behaviour of dough constituents and compute the stress involved. One mechanical model suited to both gluten and starch during bread dough baking is the "gel" model proposed by Gabriele et al. (2001) and applied by Ng et al. (2006), although others have considered starch to be visco-plastic (Mohammed et al., 2013). A "gel" turns from liquid to solid and makes it possible to mimic phase transitions such as the starch gelatinization and protein denaturation that occur during dough baking. This "gel" material can be modelled using time-dependent models such as the Lodge or Maxwell models using either infinitesimal or finite strain.

Views differ on the interactions between starch and gluten. Gluten and starch are known to be chemically incompatible materials and should therefore have limited interactions and should slide along each other (Eliasson and Larsson, 1993). Nevertheless, some authors have reported a number of interactions at the gluten-starch interface in dough (He and Hoseney, 1992; Mohammed et al., 2013; Petrofsky and Hoseney, 1995; Van Vliet et al., 1992), in bread crumb and starch-based biopolymer composites (Guessasma et al., 2015). There is hence no definitive view on the nature of the interactions between gluten and starch in bread dough during baking. To enable the simulation of all possible interactions, Mohammed et al. (2013) used a thin elastic layer that made it possible to simulate either non-cohesive or cohesive interactions at the gluten-starch interface. Such a tool will be likewise be used and further described in this study.

There are few works on the numerical modelling of GCW extension at the scale of dough constituents. Mohammed et al. (2013) examined the average stress values in a large number of rheological tests using finite elements and periodic conditions at this scale. It is interesting to note that, unlike the literature and associated modelling for dough rheology, these authors considered dough to be a heterogeneous material composed of gluten, starch and the interface between the two. Unfortunately, stress concentrations and possible locations for rupture initiation in GCWs at strain rates relevant to bread during baking were beyond the scope of their study.

Following on from the work carried out by Mohammed et al. (2013), the overall objective in the current study was to extend the microscale approach adopted in dough rheology in terms of the types of law applicable to the mechanical behaviour of dough constituents and the starch fractions, strain-rate range, and variations in the mechanical properties of dough constituents associated with the baking process. Two modelling approaches for the mechanical behaviour of bread dough were compared: linear viscoelasticity (infinitesimal strain) and visco-hyperelasticity (finite strain). This work will subsequently be completed by an analysis of the sensitivity of the computed stress to some of the model's input parameters. In the current study, the process of experimental verification has begun and has been taken as far as possible given the extreme scarcity of input data to feed the model. For this purpose, the average computed stress was compared with the very small amount of experimental data available from the literature for measurements taken at low strain rates on bread dough at ambient temperature. The simulations of the GCW extension were run in two configurations where the starch is stiffer than the gluten and two where the opposite is the case, being representative of the beginning and end of baking, before and after the starch gelatinizes and the proteins denature. The most likely locations for rupture to be initiated within the GCW for these temporally defined configurations, with and without gluten-starch interactions, were analysed through reference to stress fields using the stress triaxiality concept.

2 Materials and methods

2.1 Geometries

2.1.1 Estimation of starch fraction in the GCW at the beginning of baking

At the end of proving, the average GCW thickness in wheat dough is 240 µm (Besbes et al., 2013; Turbin-Orger et al., 2012) with an average starch fraction of around 46% v.v (Mohammed et al., 2013). However, the present work focuses on the small proportion of GCWs with a thickness of around 10-15 µm (the average thickness of the largest starch granules) as these are the most likely to rupture (Grenier et al., 2021). To the best of our knowledge very few reports of very thin GCWs in dough are available in the literature, and the present study has processed the microscopic images provided by Sandstedt (1954) that were taken at the end of baking (Fig. 1). The starch fraction was identified by measuring the areas occupied by starch and gluten in the images (Image J, National Institutes of Health, USA). The starch fraction, expressed in m^2 of starch per m^2 of GCW, was found to be 33% for image c in Fig. 1 and may slightly decrease as the GCW becomes thinner, attaining lower values locally where the starch granules are beginning to move apart (see, for example, those shown inside the green box in Fig. 2.a). Very low starch fractions (such as the 8% reference value selected for the present work) are extreme occurrences and are encountered only within strings or strands in bread crumb adjacent to locations where rupture occurs (Stokes and Donald, 2000). The choice of such a low starch fraction for the reference simulation was also intended to facilitate computation at the practical stages of the work and to allow a high strain level to be reached without impeding the location of stress concentrations in the final stages of the work. The fraction was then increased to 11%, 16% and 28% in order to take into account the range of thinner GCWs ready to rupture and to arrive at a closer approximation of the starch fraction reported in the literature in thin GCWs at the end of proving. In the geometries, the starch fraction was increased by adjusting the gluten dimensions (length and width).

2.1.2 Reference simulation

For the reference simulation, the starch fraction was set to 8% v/v because this is the fraction found at the thinnest locations within thin GCWs likely to rupture (Fig. 2.a). Where a GCW is so greatly extended the longest dimension of the starch granule is already aligned within the gluten strip (Bloksma, 1990). The single large and lenticular (A-type) starch granule in cross section measured 10 µm (long half-diameter) by 5 µm (short half-diameter). It was contained within a continuous gluten strip of 100 µm in length (L) and 20 µm wide (l) (Fig. 2.b).

2.1.3 Comparison with published experimental results

A second 2D geometry was used to compare the computed average stress values with published data at the scale of a continuous dough (section 3.1.3). The geometry was that of a cylinder of dough of 3.75 mm in height and 7.5 mm in diameter and corresponded to that used in Ng et al. (2006) (Fig. 2.c). Axisymmetry was also considered (Fig. 2.d).

A third and last 3D geometry (not shown) containing an A-type starch granule (a = 5 µm, b = c =10 µm) within a gluten strip of 100 µm length, 40 µm width and 20 µm thickness was used only once to check whether the results in 2D were relevant to those in 3D (see section 3.1.1.).

2.2 Governing equations

2.2.1 Linear viscoelasticity

The momentum balance for the quasi-static mechanical equilibrium is given by Eq. 1.

$$\boldsymbol{\nabla}.\mathbf{S} = 0 \quad (1)$$

The total stress tensor $\mathbf{S}$ is broken down into a purely elastic part and a viscoelastic part as follows (Eq. 2).

$$\mathbf{S} = \boldsymbol{\sigma} + \boldsymbol{\tau} \quad (2)$$

where $\boldsymbol{\sigma}$ is the tensor (Eq. 3) which describes the time-independent elastic behaviour and $\boldsymbol{\tau}$ the viscoelastic stress tensor which depends on the strain history of the material.

$$\boldsymbol{\sigma} = \mathbf{C}:\boldsymbol{\varepsilon} \quad (3)$$

where $\mathbf{C}$ is the fourth-order tensor of elasticity and $\boldsymbol{\varepsilon}$ is the linear strain tensor (Eq. 4).

$$\boldsymbol{\varepsilon} = \frac{1}{2}(\boldsymbol{\nabla}\mathbf{u} + (\boldsymbol{\nabla}\mathbf{u})^{\mathbf{T}}) \quad (4)$$

where $\mathbf{u}$ is the displacement. The viscoelastic stress tensor $\boldsymbol{\tau}$ is derived from the constitutive equation of the 1-element generalized Maxwell equation (Eq. 5).

$$\boldsymbol{\tau} + \lambda_r\dot{\boldsymbol{\tau}} = \lambda_r G\dot{\boldsymbol{\gamma}} \quad (5)$$

where λ_r is the relaxation time (gluten or starch), $\dot{\boldsymbol{\gamma}}$ is the infinitesimal shear strain rate tensor and G the shear elastic modulus (gluten or starch).

2.2.2 Visco-hyperelasticity

The momentum balance equation in the case of hyperelasticity is written as Eq. 6.

$$\nabla.\,(\mathbf{FS})^{\mathrm{T}} = 0 \tag{6}$$

where $\mathbf{F} = \mathbf{I} + \nabla\mathbf{u}$ is the deformation gradient where $\mathbf{I}$ is the second-order unit tensor and $\mathbf{u}$ is the displacement. $\mathbf{S}$ is the second Piola-Kirchoff stress tensor (Eq. 7). It is derived from the strain energy density function (W).

$$\mathbf{S} = 2\,\frac{\partial \mathrm{W}}{\partial \mathbf{C_c}} = \mathbf{S}_{\mathrm{el}}^{\infty} + \mathbf{Q} \tag{7}$$

where $\mathbf{C_c} = \mathbf{F^T F}$ is the right Cauchy-Green deformation tensor (Eq. 8). The elastic stress tensor is given by Eq. 8.

$$\mathbf{S}_{\mathrm{el}}^{\infty} = \mathbf{S}_{\mathrm{vol}}^{\infty} + \mathbf{S}_{\mathrm{iso}}^{\infty} = \det(\mathbf{F})^{-1}\,\mathbf{F}(\mathbf{C}\colon\boldsymbol{\varepsilon})\mathbf{F}^{\mathbf{T}} \tag{8}$$

where $\mathbf{S}_{\mathrm{vol}}^{\infty}$ and $\mathbf{S}_{\mathrm{iso}}^{\infty}$ are the volumetric and isochoric part, respectively (Holzapfel et al., 2000). The non-linear strain $\boldsymbol{\varepsilon}$ is given by Eq. 9.

$$\boldsymbol{\varepsilon} = \frac{1}{2}\left((\nabla\mathbf{u})^{\mathbf{T}} + \nabla\mathbf{u} + (\nabla\mathbf{u})^{\mathbf{T}}.\nabla\mathbf{u}\right) \tag{9}$$

The stress in the 1-element viscoelastic generalised Maxwell model is obtained from Eq. 10.

$$\mathbf{Q} + \lambda_{\mathrm{r}}\dot{\mathbf{Q}} = \lambda_{\mathrm{r}}\beta\dot{\mathbf{S}}_{\mathrm{iso}}^{\infty} \tag{10}$$

The dimensionless coefficient $\beta > 0$ denotes the strain energy factor and is written as Eq. 11.

$$\beta = \mathrm{E_{visco}} \,/\, \mathrm{E}_{el} \tag{11}$$

where $\mathrm{E_{visco}}$ and E_{el} denote the Young modulus in the viscous branch (time-dependent elasticty) and purely elastic branch (time-independent elasticity) respectively in the 2-branch Maxwell model.

In this study, the Neo-Hookean model is used for the strain energy density function (Eq. 12).

$$\mathrm{W} = \frac{1}{2}\mu(\mathbf{I_1} - 3) \tag{12}$$

where μ is the Lamé coefficient (shear modulus) and $\mathbf{I_1} = \mathrm{tr}(\mathbf{C})$ is the first invariant of the left Cauchy–Green tensor.

2.3 Initial conditions and boundary conditions

It was assumed that there was initially no stress within either the gluten or the starch. Conclusions on how the stress is concentrated will not be affected, even if that assumption does not stand, provided that discussion is limited to stress increases and to the identification of locations where these are greatest. The comparison to given yield stress cannot, however, be guaranteed.

2.3.1 Reference simulation

Strain rates of the order of 10^1 to 10^2 s^{-1} (Weegels et al., 2003) have been estimated within gas cell membranes during failure in bread dough during proving at 34°C. These strain rates are relevant to the study of crack propagation and increase in size of a hole within the GCW once a crack has been initiated. In the present study, we only focused on stress concentration before rupture. The extension of the still un-cracked GCW is hence driven by the growth of the gas cells between which it is sandwiched. At the end of proving and during baking, GCWs, before rupture, typically undergo strain rates ranging from 10^{-4} to $5 \times 10^{-3}\, s^{-1}$ and Hencky strain above 1 (Dobraszczyk, 2017; Eliasson and Larsson, 1993; Turbin-Orger et al., 2015). The strain rate depends on the GCW location within the loaf and decreases during baking. For the reference simulation, a typical decrease in strain rate at the core of the dough (Lucas et al., 2020) from $3 \times 10^{-3}\ s^{-1}$ to $1.15 \times 10^{-3} s^{-1}$ was used. The displacement $u\left(x, \pm\frac{L}{2}\right)$ was applied accordingly at the upper and lower boundaries (Eq. 13).

$$u\left(x, \pm\frac{L}{2}\right) = \frac{L}{2}\, \dot{\varepsilon}(t = 0)\, t \tag{13}$$

where $\dot{\varepsilon}(t = 0)$ is the initial strain rate ($3 \times 10^{-3}\ s^{-1}$) and t is the current time. The left and right-hand sides of the GCW are free to move (Fig. 2.b).

2.3.2 Comparison with published experimental results

In order to compare the simulations with published experimental results for the cylindrical geometry (Ng et al., 2006), a constant strain rate was applied. Upper and lower boundary displacements were accordingly applied to match the conditions used in the experiment (Eq. 14). The right-hand side of the cylinder was free to move and there was no displacement on the axis of symmetry (Fig. 2.d).

$$u\left(x, \pm\frac{L}{2}\right) = \frac{L}{2}\left(e^{\dot{\varepsilon}(t=0)t} - 1\right) \tag{14}$$

2.3.3 The gluten-starch interface: the Thin Elastic Layer (TEL)

Gluten-starch interaction at the gluten-starch interface was modelled using a Thin Elastic Layer (TEL) boundary condition. The thickness of a very thin layer can easily be defined without taking specific areas into account, the thickness e of the water phase at the gluten-starch interface being of the order of hundreds of nanometers at most. The TEL decouples the displacements on the two sides of the boundary. The interface is characterized by the two elastic constants k_n and k_t, in normal (Eq. 15) and tangential (Eq. 16) directions respectively.

$$k_n = \frac{E_{int}(1-\nu_{int})}{e(1+\nu_{int})(1-2\nu_{int})} \tag{15}$$

$$k_t = \frac{G_{int}}{e} \tag{16}$$

where ν_{int} is Poisson's ratio, E_{int} is Young's modulus and G_{int} is the shear modulus of the material at the interface. The interaction between gluten and starch was cohesive when E_{int} was set to 10^6 Pa and non-cohesive when it was set to 10^{-6} Pa.

2.4 Material properties

2.4.1 Reference properties

Both gluten and starch were considered to be viscoelastic. As neither gluten nor starch was assumed to exhibit much time-independent elasticity, the time-independent Young's modulus was set to 10 Pa. Little information on this time-independent elasticity is to be found in the literature, where discussion of the residual stress shown in the experimental data is limited. In the present work, the mechanical behaviours of both gluten and starch were mostly controlled by their time-dependent elasticity as it relaxed. At the beginning of baking, gluten is highly deformable while starch granules are non-deformable at the gas pressure values relevant to baking. As the temperature increases above the range 70-80°C, gluten denaturation and subsequent cross-linking are accompanied by an increase in gluten Young's modulus (Grenier et al., 2021) (Fig. 3). By contrast, the uptake of water by starch granules and the associated phase transitions of starch upon heating are accompanied by a decrease in the rigidity of the starch granules. In excess water, starch granules lose their integrity even under gentle shearing, the temperature at which this transition occurs varying with the starch type. Mechanical testing of individual starch granules immediately after heating in excess water has shown that potato starch granules can become highly deformable at pressures of the order of hundreds of Pa (Carrington et al., 1998; Desse et al., 2010; Fisher et al., 1997). At the levels of hydration relevant to bread dough, the extent of granule softening remains uncertain. Microscopic observations of GCWs revealed that the granules appeared to have flattened significantly in wheat bread crumb (Sandstedt, 1954) and to an extreme extent in bread prepared with low-amylose starch which is reputed to soften/disrupt wheat starch at an earlier point than usual during heating (Kusunose et al., 1999). Where baking occurs at atmospheric pressure, the release of carbon dioxide in gas cells becomes limited in the range of temperatures (above 60-70°C) at which granule softening is likely to occur. This makes it highly improbable that GCWs will reach any great degree of extension in these conditions and there is therefore no sense in studying high levels of extension for such cases. It is relevant to do so, though, for innovative baking processes such as partial vacuum baking (Grenier et al., 2019; Lucas et al., 2016; Rondeau-Mouro et al., 2019; Şimşek, 2020) where extension is forced at mid-baking by the decrease in pressure in the oven's atmosphere. This decrease in pressure is accompanied by water ebullition and gas extension and, consequently, GCW extension is enhanced in these conditions.

Two sets of Young's moduli were therefore considered for the computations. The first relates to early baking (before 50-60°C is reached) when the starch (100 kPa) is more rigid than the gluten (10 kPa) (Attenburrow et al., 1990; Dreese et al., 1988; Khatkar and Schofield, 2002; Mohammed et al., 2013), and the second reflects the conditions of advanced baking (beyond 70°C) when gluten has low deformability (100 kPa) (Attenburrow et al., 1990) and starch deformability is high (10 kPa) (Fisher et al., 1997) (Fig. 3). The orders of magnitude for the first set derive from the work of Mohammed et al. (2013) and are simply inverted to form the second set because no data for wheat starch at moderate levels of hydration and high temperatures is available in the literature. For the reference simulation, the same relaxation time (10 s) was used for both gluten and starch. These parameters are assumed to remain constant throughout the extension (Fig. 3). All parameters are gathered in Table 1.

2.4.2 Comparison with published experimental results

Since the dough was treated as uniform in the experiment used for validation, the mechanical properties were also considered to be uniform throughout the dough cylinder for that specific case. The average Young's modulus of the dough (100 kPa) was chosen. Two relaxation times (10 and 100 s) were also used in order to evaluate the sensitivity of the average stress to strain rate.

2.5 Digital modelling

Finite element computations were carried out using the COMSOL Multiphysics® v. 5.4 (COMSOL AB, Stockholm, Sweden) MUMPS solver . A mesh convergence test was run to find the best balance between simulation time/use of computer resources and the stability of the model. The average run time varied from 10 minutes to 1 day on an Xeon (R) W-2155 CPU Intel processor at 3.31 GHz, with 256 Go RAM.

2.6 Analysis of stress fields and the triaxiality factor

For stress analysis, the von Mises criterion was applied (Eq. 17). This equivalent tensile stress (known as von Mises stress, σ_{vm}) is that most commonly used for the analysis of yielding in materials science.

$$\sigma_{vm} = \sqrt{\frac{(\sigma_{11}-\sigma_{22})^2+(\sigma_{22}+\sigma_{33})^2+(\sigma_{33}+\sigma_{11})^2+6({\sigma_{12}}^2+{\sigma_{23}}^2+{\sigma_{31}}^2)^2}{2}} \quad (17)$$

The triaxiality factor ($T.F.$, Eq. 18) was also used to identify the regions of uniaxial extension and shear. When the triaxiality factor is around 0.33 the material is mostly uniaxially extended and when it is equal to zero the material is mostly sheared. In the stress, the numbers refer to the direction of the space. The first number is the direction normal to the surface upon which the stress is applied and the second is the direction of the component of the stress.

$$T.F. = \frac{\sigma_{eq}}{\sigma_{vm}} \quad (18)$$

where $\sigma_{eq} = \frac{1}{3}\,(\overline{\overline{\sigma}}) = \frac{1}{3}(\sigma_{11} + \sigma_{22} + \sigma_{33})$

3 Results and discussion

3.1 Model analysis and experimental validation

Average stress values computed using linear-viscoelasticity in 2D and 3D were compared in order to check that the agreement between them was sufficient for the entire study to be conducted using 2D geometries (section 3.1.1). Viscoelasticity and visco-hyperelasticity approaches were then compared to assess where visco-hyperelasticity was more suited to the task than linear viscoelasticity (section 3.1.2). Last, the average stress values computed using hyperelasticity were compared to previously published experimental data (Ng et al., 2006) (section 3.1.3).

3.1.1 Comparison between 2D and 3D geometries

Fig. 4 shows the average values for von Mises stress vs Hencky strain in 2D and 3D geometries using the reference simulation for the two selected cases (starch granule more rigid than gluten/gluten more rigid than starch granule) (Fig. 4). Where the starch granule was more rigid than the gluten and up to a Hencky strain of 0.67, the difference when using linear visco-elasticity in 2D and 3D did not exceed 2%. Where the gluten was more rigid than the starch granule, this difference reached the order of 20% at most. These discrepancies are in line with those reported by Mohammed et al. (2013). 2D rather than 3D geometry was therefore used to reduce computation times without too greatly distorting the results.

3.1.2 Comparison between linear viscoelasticity and visco-hyperelasticity

The average values for von Mises stress vs Hencky strain up to 0.67 are shown in Fig. 5 for both linear viscoelasticity and visco-hyperelasticity. There was good agreement between simulations up to a strain of 0.08. Thereafter, the average stress values diverged. It is notable in Fig. 5 that, when E_{starch}/E_{gluten}=0.1, the viscoelasticity model barely registers the strain softening observed experimentally by Ng et al. (2006) at low strain rates. For this reason, we selected the visco-hyperelasticity model for the next steps of the study.

3.1.3 Comparison with published experimental results

The average von Mises stress values computed using the axisymmetric geometry were compared to published experimental results obtained at ambient temperature from dough (Ng et al., 2006). The objective here was solely to validate the structure of the model. It is impossible to achieve greater quantitative validation because the mechanical properties used in the model are unlikely to have been exactly those of the dough used in the experiment. Fig. 6 shows both simulated and experimental average values for stress vs Hencky strain at different strain rates (0.3 s^{-1} and 0.003 s^{-1}). At the high strain rate (0.3 s^{-1}), no good quantitative agreement could be found between the simulations in the present study and the experiments reported in the literature (Fig. 6.a). This is probably due to an overestimate of the Young's modulus. There is unfortunately no guarantee that the elasticity of the dough used by Ng et al. (2006) in their experiment was not lower than that used in the simulation. However, similarities in strain-hardening were observed between the simulation and the experiment performed by Ng et al. (2006) and the stress exhibited almost no sensitivity to relaxation time (Fig. 6.a). Elasticity was the main driver for the stress in this high strain rate configuration. At the low strain rate (0.003 s^{-1}), when the model was less sensitive to elasticity and far more so to viscosity, a quite good quantitative and qualitative agreement was found between the simulations and the experiments (Fig. 6.b). As expected, the average von Mises stress values within the GCW were strongly dependent on the relaxation time at this low strain rate (Fig. 6.b). This indicates that the estimation of the relaxation time for dough (or dough constituents) has to be quite accurate when addressing GCW extension during proving or bread baking, since it is the viscous aspect of the dough that mostly drives the stress under such low strain rate conditions. Note that this statement is only true if the assumption of very low time-independent elasticity was true. At low strain rates, precisely the opposite conclusions would be drawn if there were a degree of time-independent elasticity in the dough. In such a case, only time-independent elasticity would be relevant because all possible time-dependent elasticity relaxation would have already occurred.

3.2 Average stress values

3.2.1 Reference starch fraction

Fig. 7 plots the average values of von Mises stress as a function of the Hencky strain for starch to gluten moduli ratios of 0.1 and 10. The starch-gluten moduli ratios were found to have significant impact on the average von Mises stress. Average stress values where starch was less rigid than gluten were tenfold higher than those where starch was more rigid than gluten. This was largely due to the high proportion of gluten, which accounted for 92% of the total volume.

The nature of the interactions between gluten and starch was found to have no effect on the average von Mises stress within the GCW for the reference starch fraction (8%). This does not fit with the reported results of Mohammed et al. (2013), who found that the cohesive/non-cohesive nature of the gluten-starch interface affected average stress values in every case tested in their study. The difference is explained by their choice of starch fraction, which averaged around 46 % in bulk dough without gas cells (Mohammed et al., 2013; Tanner et al., 2011). The following section will address the different starch fractions and will extend the comparison with the data reported by Mohammed et al. (2013).

3.2.2 Effect of starch fraction

Fig. 8 shows the average von Mises stress as a function of Hencky strain for the reference (blue color) starch fractions of 11, 16 and 28% and compares the cohesive and non-cohesive hypotheses concerning the interface between starch and gluten; only the case where the starch is more rigid than the gluten is considered here. The nature of the interaction increasingly affected average von Mises stress values as the starch fraction increased (Fig. 8). From this, it can be concluded that the nature of the gluten-starch interaction affected the average stress within the GCW as soon as the starch fraction exceeded a threshold located between 8% and 11%. As expected, the decrease in average stress values that accompanied the increase in starch fraction was greater when the interface was non-cohesive. Slightly greater average stress values were found when a cohesive interface was involved. Indeed, within the area of gluten closest to the starch granule, the increase in starch fraction was accompanied by a greater increase in stress values because the gluten in this area was under greater strain than it was when the interface was non-cohesive.

3.3 Stress fields and triaxiality: stress concentrations in early and late baking

The objective in this section is to refine the foregoing analysis by considering local stresses rather than average values. The intention is to learn more about the most likely locations for GCW rupture in the different configurations. From this point on, we will adopt the working assumption that the locations with the highest concentrations of stress are where the rupture of the material (the GCW in this instance) is most likely to be initiated. In other words, we assume that rupture occurs when the yield stress value is exceeded. In a further step, this analysis will make use of these findings to predict the phenomena most likely to be present in microscopic observations of the GCW in baked bread crumb. It should be remembered that the range of moduli ratios that have been tested in the course of the present work are also of significance to the baking process and to gradual changes in molecular conformation upon heating, as detailed in section 2.4.1.

Fig. 9 and Fig. 10 show von Mises stress fields for starch fractions of 8% (reference fraction) and 28% at 0.67 and 0.4 Hencky strains respectively, for different starch-gluten modulus ratios (0.1 and 10) and for cohesive/non-cohesive interactions. We next provide the refined analysis referred to above for the reference fraction. The locations of stress concentrations in the 28% starch fraction were found to be identical to those in the reference fraction. Only the magnitude of stress and strain (0.41) before modelled failure differed.

3.3.1 Early baking, $E_{starch} > E_{gluten}$

Fig. 9 a depicts results when the starch granule is more rigid than the gluten for the two gluten-starch interface types: cohesive (left) and non-cohesive (right).

Where it was assumed that the interaction at the gluten-starch interface is cohesive, the starch granule reinforced the gluten film and the stress spread through the entirety of the gluten and starch by means of the cohesive interaction (Fig. 9.a, on the left-hand side). The rupture was most probably initiated at two points of extreme stress within the gluten film; one lying a few micrometres away from the starch granule in the direction of the extension within the gluten and another immediately adjacent to the rim of the granule (see arrows in Fig. 9.a, left). The maximum stresses were 1.8×10^3 Pa and 2.08×10^4 Pa for the cohesive and non-cohesive gluten-starch interfaces respectively and were thus separated by an order of magnitude. It is worth remembering that yield stress magnitudes in dough for low strain rates (0.1 s^{-1}) ranged from 0.5 to 1.1×10^3 Pa depending on the quality of the gluten network (Attenburrow et al., 1992; Chin and Campbell, 2005; Dunnewind et al., 2003). Such a thin GCW containing a still-rigid starch particle is likely to have ruptured at a lower Hencky strain than 0.67. This would be all the more probable if a certain amount of stress had been previously stored in the GCW at the beginning of the extension process, as can be expected to occur in proven dough at the beginning of baking.

Fig. 9 also shows the triaxiality factor fields that provide information on those areas where unidirectional extension (Fig. 9.c) and shear (Fig. 9.e) occur (cohesive hypothesis shown on left). In those cases where the gluten-starch interface was cohesive, the uniaxial extension within the gluten was strongest close to the rims of the starch granules and spread along the sides of the granules (Fig. 9.c, left). Shear was also found within the gluten in the upper and lower regions close to the gluten-starch interface. This shearing probably increases the likelihood that the interface will rupture at these locations. If the cohesive assumption is valid, these simulations tell us that microscopic observations should reveal gluten in close contact with the starch at the mid-point of the granule's length and gluten shreds near the edges of the granule.

By contrast, non-cohesive interactions at the gluten-starch interface caused a concentration of stress that was largely confined to the gluten lying in the direction of the extension close to the very edge of the starch granule (Fig. 9.a, right). This was where the greatest uniaxial extension of the gluten film occurred (Fig. 9.c, right). It was also the point at which the GCW was most likely to rupture. The starch granule did not reinforce the gluten as it had done in the previous case and stress within the granule was much lower (see Fig. 9.b vs 9.a). In this hypothesis, once initiated, rupture will spread within the gluten and is then expected to slide around the starch granule since there is no interaction at the gluten-starch interface. Stress values were also high in the gluten film that was close to the lateral edge of the starch granule (Fig 9.a, right) and this constitutes a second highly plausible location for rupture to occur (see arrow in Fig. 9). If the non-cohesive hypothesis is valid, these simulations tell us that, taking into account the uncertainty as to the degree of slippage, the starch granules located closest to the point of rupture might be partially covered with gluten but, unlike those in the cohesive model, they should be totally free of gluten shreds at their edges.

3.3.2 Late baking, $E_{starch} < E_{gluten}$

Fig. 9.b shows von Mises stress fields at 0.67 Hencky strain when the starch granule was less rigid than the gluten for cohesive (left) and non-cohesive (right) gluten-starch interfaces. When it was sufficiently soft, the starch granule became elongated in the direction of the extension and the stress became concentrated along the lateral surfaces of the starch granule because of the extreme extension of the gluten along both sides of the granule (Fig. 9.b and d, green arrows). The rupture of the gluten was most likely to occur along the surface of the granule where both strain and stress were at their greatest. Here again, with a non-cohesive gluten-starch interface, the surface of the starch granule should be free of gluten following rupture. With a cohesive gluten-starch interface, some gluten should remain on the lateral surfaces of the starch granule. In the direction of extension, the stress decreased with distance from the starch granules. It is possible that he gluten that had previously been strained in these areas when it had been less rigid than the starch (replicating the early stage of baking, see section 3.3.1) had now been attenuated by the elongation of the starch granule and the stress redistributed between the gluten and the starch. Such a change is likely to increase the extensive capacity of the GCW but only if starch granule softening occurs before the gluten has become too stiff. We should note that these two events are not well documented in the literature. Note also that if granule softening were to occur very early in the baking process it is possible that the GCWs might rupture far less frequently, leading to an incomplete opening of the porous structure of the bread’s crumb. This would cause the baked dough to shrink during the cooling step. Again, this transition cannot be analyzed further without information on the evolution of the starch modulus during the heating process.

This analysis has also revealed that the main difference found between cohesive and non-cohesive interactions at the gluten-starch interface was an element of shear on the side of the granule where cohesive interactions were involved but none where interactions were non-cohesive (Fig. 9.f, left vs right). This explains why the stress spread throughout the starch and gluten and why the maximum stress remained lower than when the gluten-starch interactions were non-cohesive. In this case, the triaxiality factor showed that uniaxial extension and shear mostly decreased with distance from the granule, following the direction of the decrease in stress (Fig. 9.d and f).

3.3.3 About the incompressibilty of the starch granule

The conclusions drawn up to this point rely on the hypothesis of incompressibility of the starch granule. Unfortunately we found no literature dealing with Poisson's ratio of starch granule to sustain the hypothesis of incompressibily. In order to identify how far the non validity of the assumption of starch incompressibility could affect the results, simulations were run using Poisson's ratio of 0.3, which is an extreme value for polymers (see supplementary material 1). On the one hand, previous conclusions on the location where the stress concentrates the most were unchanged. On the other hand, the effect of cohesion/non-cohesion between gluten and starch on the mean von Mises stress decreased with decreasing Poisson's ratio. This effect was almost totally cancelled (remaining difference of 2.5%) in the late baking configuration and was quite reduced (-20%) in the early baking configuration, where the starch granule was more rigid than gluten.

Conclusion and future research

Both linear viscoelastic and visco-hyperelastic models were assessed to determine their suitability for the computation of average stress and of stress fields during uniaxial extension within gas cell walls (GCWs) in bread dough during baking. Comuptation of visco-hyperelasticity involving finite strain was found to be more suited to the task of replicating GCW extension under strain and strain rates close to those encountered during baking. The visco-hyperelasticity model made it possible to describe strain-hardening in sufficient accordance with experimental results (Dobraszczyk; Ng et al., 2006; Van Vliet et al., 1992) for a high strain rate ($\dot{\varepsilon} = 3.10^{-1}s^{-1}$). Strain softening was computed at low Hencky strain for a low strain rate ($\dot{\varepsilon} = 3.10^{-3}s^{-1}$) in line with the work of Ng et al. (2006). The simulations also demonstrated that proper identification of relaxation times is important for the analysis of low strain rates such as those encountered during baking provided that not too much time-independent elasticity is involved.

It was found that the nature of gluten-starch interactions had no significant effect on the average stress for the low starch fraction used as a reference (8%). Whether the gluten-starch interaction was cohesive or non-cohesive did, however, become significant when the starch fraction was increased. For a starch granule fraction of 28%, which was the closest to that reported in the literature for thin GCWs and which was estimated in the present study, the mechanical interaction between starch and gluten was found to have an impact on average stress values, as already evidenced for bulk dough in the literature. The nature of the interactions between starch and gluten during baking is still a matter of debate in the cereal science community. Our simulations confirmed that information on the nature of the interaction at the gluten-starch interface such as that proposed by Jekle et al. (2016) is important for the appropriate modelling of the stress fields within GCWs. The rupture location will depend on the nature of this gluten-starch interaction which can be determined by the presence or absence of a number of gluten shreds along the surfaces of the starch granules located closest to the hole produced by the rupture. This evidence may provide a useful indicator for the future microscopic analysis of holes in the GCWs of bread crumb. This result also confirms that the interaction between starch granules and gluten may affect dough performance and that gluten and starch should be considered in interaction (Gao et al., 2020) rather than separately, as is commonly practiced in the literature. The experimental verification of the model remains insufficient, requiring further experimental work to identify the mechanical properties of dough within the relevant temperature range for baking carried out at low strain rates and in a controlled gaseous environment to reflect real-life conditions for bread dough during baking. Work should first be carried out to estimate the time-independent elasticity of the protein matrix and liquid lamella at the dough-gas interface as this might strongly affect strain-hardening at low strain rates. It is almost impossible to record the low strain rates relevant to dough proving and baking using conventional rheometers. A dedicated experimental device for bubble inflation that is capable of reproducing both low and high strain rates in an atmosphere closely resembling that encountered in gas cells during the baking of real dough must therefore be developed. Such a device would enable the elimination of doubt concerning the mechanical properties of dough at high temperatures and provide data to support the conclusions drawn in the present study. The development of this device will form the next step in our investigation. Second, the possible evolution of the interactions at the gluten-starch interface between the beginning and end of baking and the changes that are even more likely to occur between the end of baking and the end of cooling require analysis. This work is necessary for the appropriate modelling of the stress fields in GCWs during the last stages of bread making to be carried out.

Acknowledgments

The first author, Kossigan Bernard DEDEY, is the holder of a grant from Université Rennes 1 and INRAE.

References

Attenburrow, G., Barnes, D., Davies, A., Ingman, S., (1990). Rheological properties of wheat gluten. Journal of Cereal Science 12(1), 1-14.

Attenburrow, G.E., Davies, A.P., Goodband, R.M., Ingman, S.J., (1992). The fracture behaviour of starch and gluten in the glassy state. Journal of Cereal Science 16(1), 1-12.

Besbes, E., Jury, V., Monteau, J.-Y., Le Bail, A., (2013). Characterizing the cellular structure of bread crumb and crust as affected by heating rate using X-ray microtomography. Journal of food engineering 115(3), 415-423.

Bloksma, A., (1990). Dough structure, dough rheology and baking quality. Cereals Food World 35(2), 237-244.

Carrington, S., Fisher, L., Odell, J., (1998). Microrheology of Swollen Starch Granules, *Gums and Stabilisers for the Food Industry 9*. Elsevier, pp. 371-380.

Chin, N.L., Campbell, G.M., (2005). Dough aeration and rheology: Part 2. Effects of flour type, mixing speed and total work input on aeration and rheology of bread dough. Journal of the Science of Food and Agriculture 85(13), 2194-2202.

Chiotelli, E., Le Meste, M., (2002). Effect of small and large wheat starch granules on thermomechanical behavior of starch. Cereal Chemistry 79(2), 286-293.

Desse, M., Fraiseau, D., Mitchell, J., Budtova, T., (2010). Individual swollen starch granules under mechanical stress: evidence for deformation and volume loss. Soft Matter 6(2), 363-369.

Dobraszczyk, B., (2017). Dough rheology and breadmaking. Peer review: Teigrheologie / Backeigenschaften Cereal Technology 01, 4-19.

Dreese, P., Faubion, J.M., Hoseney, R.C., (1988). Dynamic rheological properties of flour, gluten, and gluten starch doughs. I. Temperature-dependent changes during heating. Cereal Chem. 65(4), 348-353.

Dunnewind, B., Sliwinski, E., Grolle, K., Vliet, T.v., (2003). The kieffer dough and gluten extensibility rig-an experimental evaluation. Journal of Texture Studies 34(5-6), 537-560.

Eliasson, A.-C., Larsson, K., (1993). *Cereals in breadmaking: a molecular colloidal approach*. Marcel Dekker, New York (USA).

Faubion, J., Dreese, P., Diehl, K., (1985). Dynamic rheological testing of wheat flour doughs.

Fisher, L.R., Carrington, S.P., Odell, J.A., (1997). Deformation mechanics of individual swollen starch granules, in: Frazier, P.J., Donald, A.M., Richmond, P. (Eds.), *Starch: Structure and Functionality* Royal Society of Chemistry, pp. 105-114.

Gabriele, D., de Cindio, B., D'Antona, P., (2001). A weak gel model for foods. Rheologica Acta 40(2), 120-127.

Gan, Z., Angold, R.E., Williams, M.R., Ellis, P.R., Vaughan, J.G., Galliard, T., (1990). The microstructure and gas retention of bread dough. Journal of Cereal Science 12(1), 15-24.

Gao, X., Tong, J., Guo, L., Yu, L., Li, S., Yang, B., Wang, L., Liu, Y., Li, F., Guo, J., (2020). Influence of gluten and starch granules interactions on dough mixing properties in wheat (Triticum aestivum L.). Food Hydrocolloids 106, 105885.

Grenier, D., Lucas, T., Le Ray, D., (2019). Enhanced aeration of part-baked bread using a novel combination of baking and partial vacuum. Journal of Food Engineering 248, 62-70.

Grenier, D., Rondeau-Mouro, C., Dedey, K.B., Morel, M.-H., Lucas, T., (2021). Gas cell opening in bread dough during baking. Trends in Food Science & Technology 109, 482-498.

Guessasma, S., Bassir, D., Hedjazi, L., (2015). Influence of interphase properties on the effective behaviour of a starch-hemp composite. Materials & Design 65, 1053-1063.

Hayman, D.A., Sipes, K., Hoseney, R., Faubion, J., (1998). Factors controlling gas cell failure in bread dough. Cereal Chemistry 75(5), 585-589.

He, H., Hoseney, R., (1992). Factors controlling gas retention in non-heated doughs. Cereal Chem 69(1), 1-6.

Herrera, M.P., Vasanthan, T., Chen, L., (2017). Rheology of starch nanoparticles as influenced by particle size, concentration and temperature. Food Hydrocolloids 66, 237-245.

Holzapfel, G.A., Gasser, T.C., Ogden, R.W., (2000). A new constitutive framework for arterial wall mechanics and a comparative study of material models. Journal of elasticity and the physical science of solids 61(1-3), 1-48.

Janssen, A., Van Vliet, T., Vereijken, J., (1996). Rheological behaviour of wheat glutens at small and large deformations. Comparison of two glutens differing in bread making potential. Journal of Cereal Science 23(1), 19-31.

Jekle, M., Mühlberger, K., Becker, T., (2016). Starch-gluten interactions during gelatinization and its functionality in dough like model systems. Food Hydrocolloids 54, 196-201.

Khatkar, B.S., Schofield, J.D., (2002). Dynamic rheology of wheat flour dough. II. Assessment of dough strength and bread-making quality. Journal of the Science of Food and Agriculture 82(8), 823-826.

Kokelaar, J.J., van Vliet, T., Prins, A., (1996). Strain hardening properties and extensibility of flour and gluten doughs in relation to breadmaking performance. Journal of Cereal Science 24(3), 199-214.

Kusunose, C., Fujii, T., Matsumoto, H., (1999). Role of starch granules in controlling expansion of dough during baking. Cereal chemistry 76(6), 920-924.

Lucas, T., Grenier, D., Le Ray, D., (2016). Facility and method for treating food products, such as cellular products, in particular for expanding said products, in: Office, E.P. (Ed.), *Espacenet*. INRAE, France.

Lucas, T., Vanin, F., Ureta, M., Challois, S., Diascorn, Y., Salvadori, V., Grenier, D., (2020). Inflation, squeezing and collapse in wheat flour dough during baking: Effects of flour quality and oven temperature. Journal of Cereal Science 95, 103017.

Mohammed, M.A.P., Tarleton, E., Charalambides, M.N., Williams, J., (2013). Mechanical characterization and micromechanical modeling of bread dough. Journal of Rheology 57(1), 249-272.

Ng, T.S., (2007). Linear to nonlinear rheology of bread dough and its constituents. Massachusetts Institute of Technology.

Ng, T.S., McKinley, G.H., Padmanabhan, M., (2006). Linear to non-linear rheology of wheat flour dough. Applied Rheology 16(5), 265-274.

Petrofsky, K., Hoseney, R., (1995). Rheological properties of dough made with starch and gluten from several cereal sources. Cereal Chemistry 72(1), 53-57.

Rondeau-Mouro, C., Godfrin, C., Cambert, M., Rouillac, J., Diascorn, Y., Lucas, T., Grenier, D., (2019). Characterization of gluten-free bread crumb baked at atmospheric and reduced pressures using TD-NMR. Magnetic Resonance in Chemistry 57(9), 649-660.

Sandstedt, R., (1954). The microscopic structure of bread and dough. Cereal Chem. 31, 43-49.

Şimşek, S.T., (2020). Evaluation of partial-vacuum baking for gluten-free bread: Effects on quality attributes and storage properties. Journal of Cereal Science 91, 102891.

Stokes, D., Donald, A., (2000). In situ mechanical testing of dry and hydrated breadcrumb in the environmental scanning electron microscope (ESEM). Journal of Materials Science 35(3), 599-607.

Tanner, R.I., Qi, F., Dai, S., (2011). Bread dough rheology: an improved damage function model. Rheologica acta 50(1), 75-86.
Turbin-Orger, A., Babin, P., Boller, E., Chaunier, L., Chiron, H., Della Valle, G., Dendievel, R., Réguerre, A., Salvo, L., (2015). Growth and setting of gas bubbles in a viscoelastic matrix imaged by X-ray microtomography: the evolution of cellular structures in fermenting wheat flour dough. Soft matter 11(17), 3373-3384.
Turbin-Orger, A., Boller, E., Chaunier, L., Chiron, H., Della Valle, G., Réguerre, A.-L., (2012). Kinetics of bubble growth in wheat flour dough during proofing studied by computed X-ray micro-tomography. Journal of Cereal Science 56(3), 676-683.
Van Vliet, T., Janssen, A.M., Bloksma, A.H., Walstra, P., (1992). Strain hardening of dough as a requirement for gas retention. Journal of Texture Studies 23(4), 439-460.
Weegels, P.L., Groeneweg, F., Esselink, E., Smit, R., Brown, R., Ferdinando, D., (2003). Large and fast deformations crucial for the rheology of proofing dough. Cereal Chem 80(4), 424-426.
Wesołowska-Trojanowska, M., Tomczynska-Mleko, M., Mazurkiewicz, J., Kwiatkowski, C., Kowalczyk, K., Sołowiej, B., Mleko, S., (2014). Rheological properties of gluten obtained from polish wheat cultivars. Bulgarian Journal of Agricultural Science 20(5), 1221-1226.

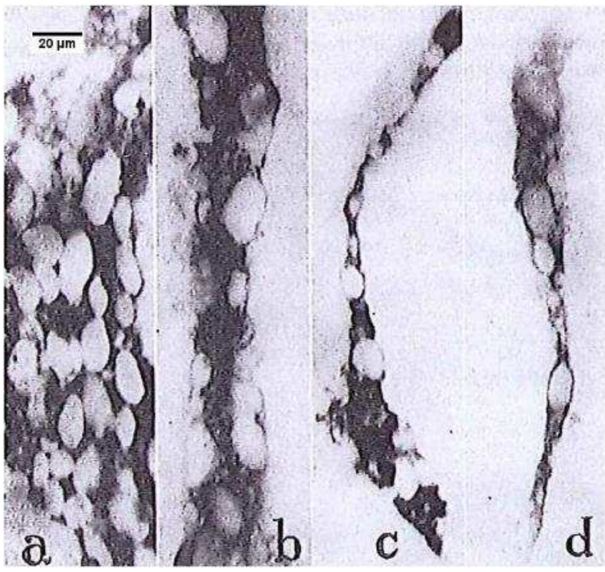

Fig. 1. Microscopic views of GCW cross-sections at the end of fermentation from Sandstedt (1954): a. thick GCW; b., c. and d. thin GCWs.

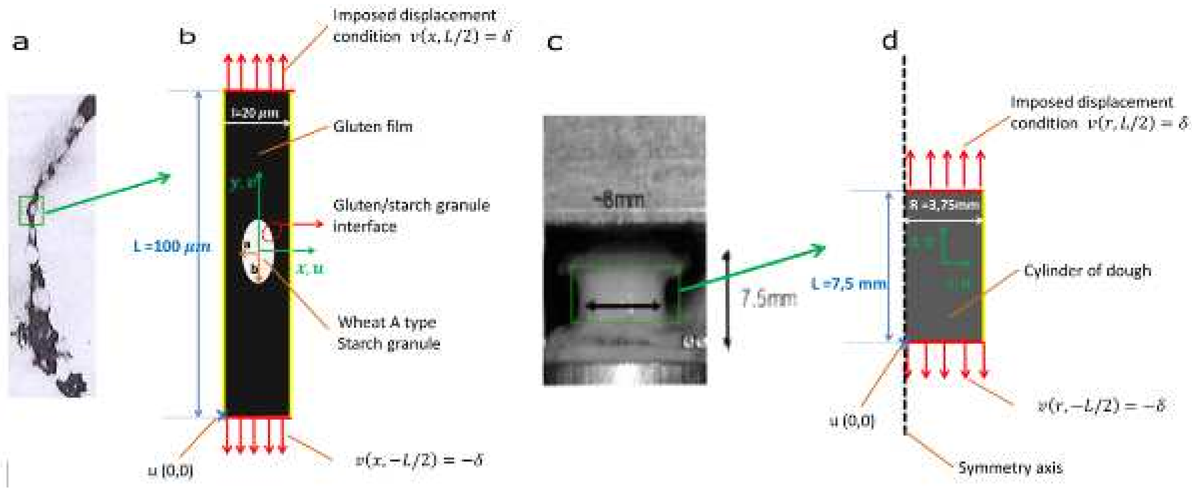

Fig. 2. Geometries and boundary conditions: a. cross-section of a gas cell wall (GCW) about to rupture at the end of proving (Sandstedt, 1954); b. 2D reference geometry for simulations; c. cylindrical geometry of filament stretching experiments in Ng et al. (2006); d. 2D axisymmetric model-validation geometry based on the filament stretching experiment shown in c.

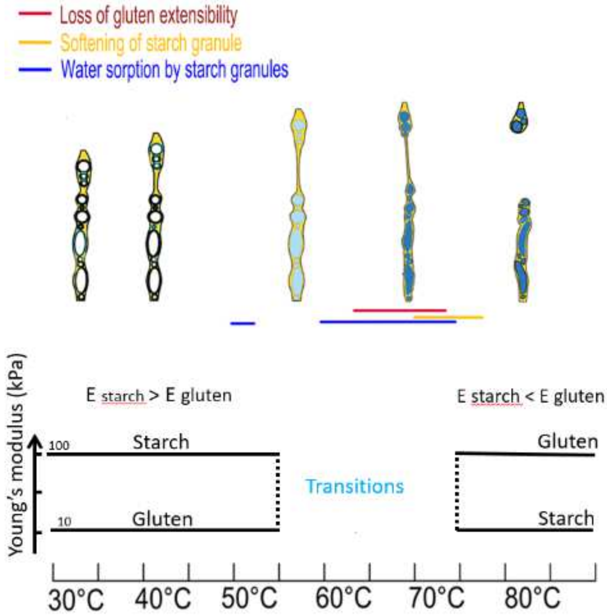

Fig. 3. Mechanical properties for T < 50-60°C, E_{starch}/E_{gluten}=10 (early in baking) and T > 70-80°C, E_{starch}/E_{gluten}= 0.1 (later in baking). The GCW spatial organisation and morphology shown in the upper part of the figure has been adapted from Grenier et al. (2021).

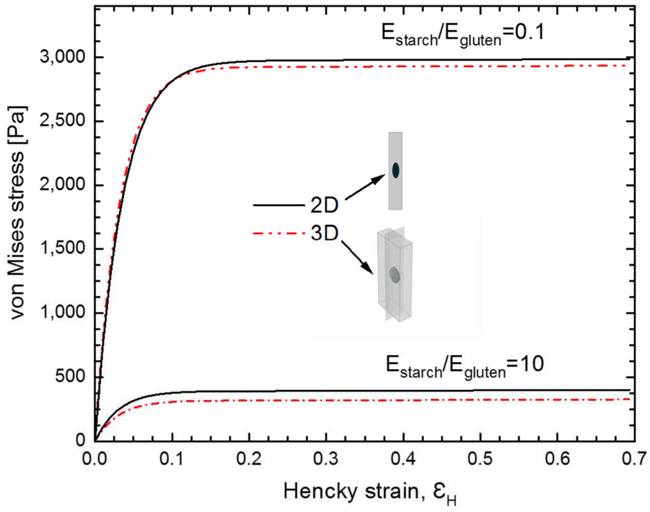

Fig. 4. Average values for von Mises stress vs Hencky strain in the case of **cohesive** interaction at the gluten-starch interface.

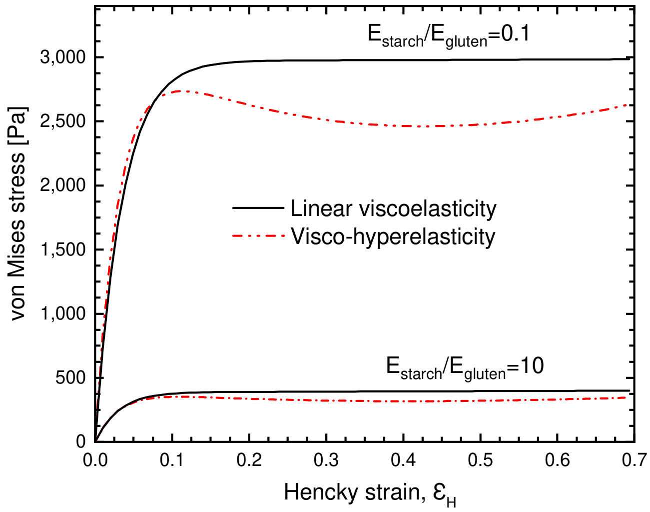

Fig. 5. Plotted average values for von Mises stress vs Hencky strain, comparing linear viscoelasticity with visco-hyperelasticity where there is cohesive interaction at the gluten-starch interface.

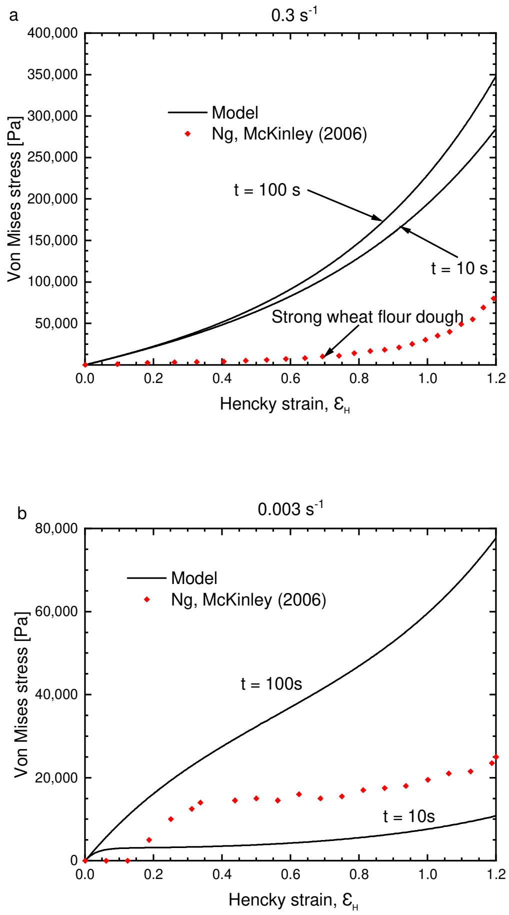

Fig. 6. Average values for von Mises stress vs. Hencky strain, comparing the proposed model with experimental data obtained at two different strain rates (0.3 s^{-1} and 0.003 s^{-1}) (Ng et al., 2006).

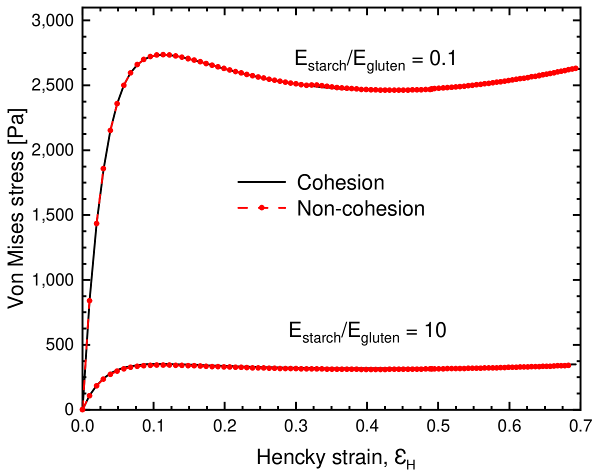

Fig. 7. Reference starch fraction – average values for von Mises stress vs Hencky strain computed with the proposed model for both the cohesive and non-cohesive gluten-starch interface hypotheses and for two different starch-gluten modulus ratios $E_{starch}/E_{gluten} = 0.1$ and $E_{starch}/E_{gluten} = 10$.

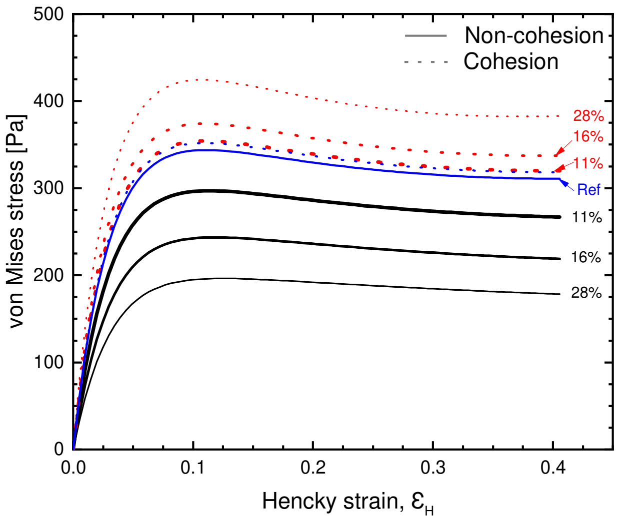

Fig. 8. Starch fractions – average values for von Mises stress vs Hencky strain computed with the proposed model, for different starch fractions (11%, 16% and 28%), the last being of relevance to GCWs in bread dough at the end of fermentation. All calculations were performed for the case $E_{starch}/E_{gluten} = 10$.

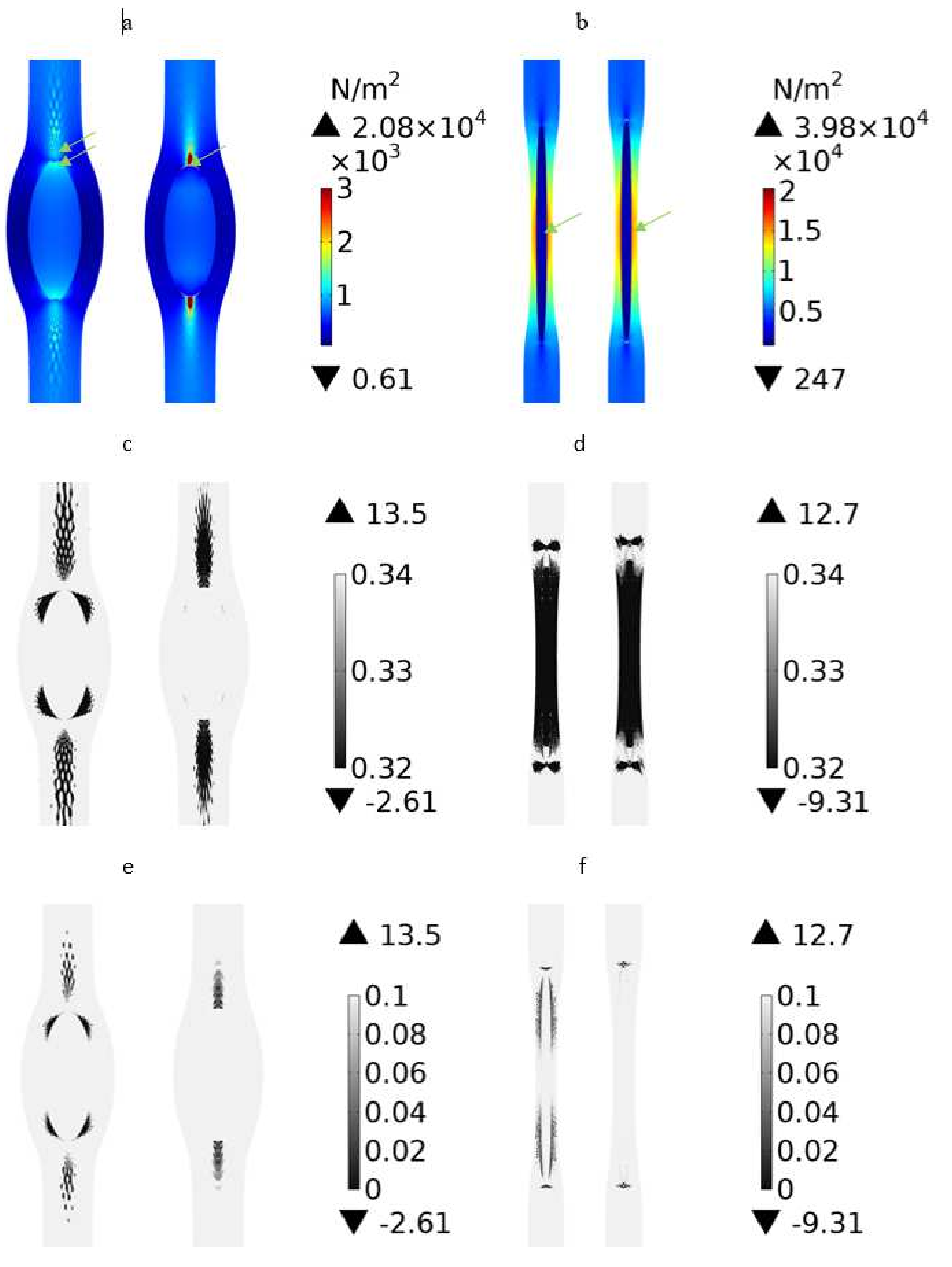

Fig. 9. von Mises stress fields within the GCW at the end of extension (0.67 Hencky Strain) for the two references $E_{starch}/E_{gluten}=10$ (a, c, e) and $E_{starch}/E_{gluten}=0.1$ (b, d, f). Triaxiality factor: uniaxial extension (TF = 0.33, c and d) and shear (TF = 0, e and f). Cohesive (left-hand image) and non-cohesive (right-hand image) gluten-starch interfaces are shown for each subplot a, b, c, d, e and f.

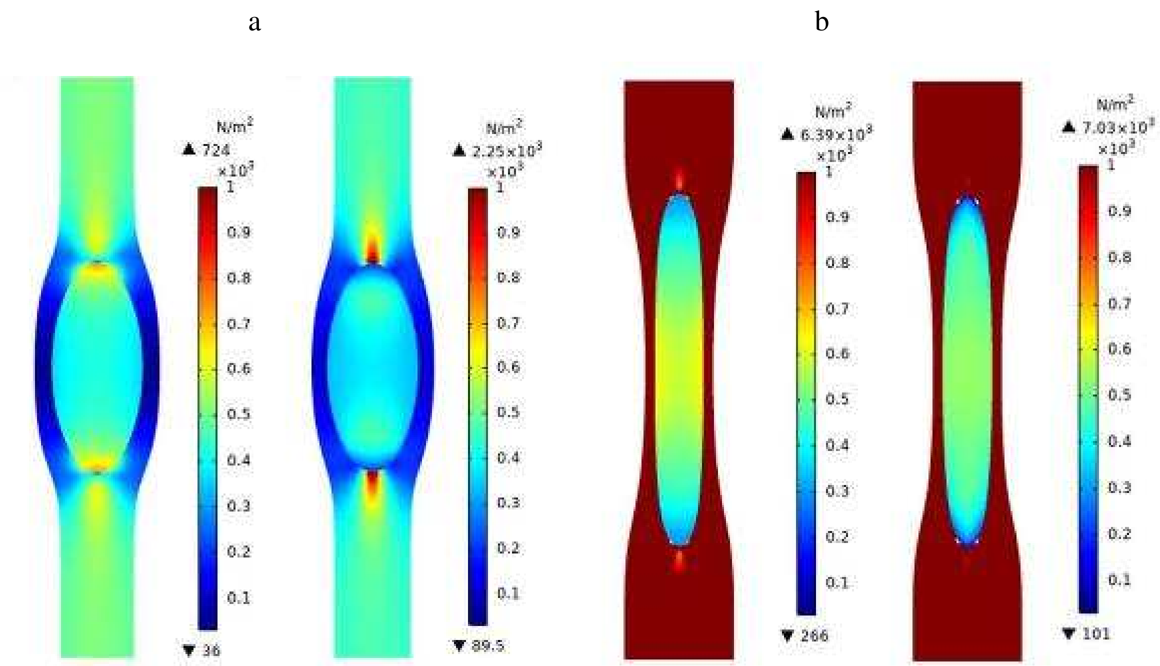

Fig. 10. von Mises stress fields within the GCW at the end of extension (0.41 Hencky Strain) for a 28% starch fraction where $E_{starch} > E_{gluten}$ (a) and $E_{starch} < E_{gluten}$ (b). Cohesive (left-hand image) and non-cohesive (right-hand image) gluten-starch interfaces are shown for each subplot.

Table 1. Nomenclature and input parameters

		Unit	Value	Ref
Letters				
a	Half of the smallest dimension of the starch granule (A-type)	m	10×10^{-6}	[6]
b, c	Half of the largest dimension of the starch granule (A-type)	m	5×10^{-6}	
$\mathbf{C}$	Fourth-order tensor of elasticity			
$\mathbf{C_c}$	Right Cauchy-Green deformation tensor			
e	Thickness of the material at the gluten-starch interface	m	1×10^{-6}	
E	Time-independent elasticity	Pa	10	
E_{gluten}	Young's modulus of gluten	kPa	T < 50-60°C : 10 T > 70-80°C: 100	[21]
E_{starch}	Young's modulus of starch		T < 50-60°C: 100 T > 70-80°C: 10	
E_{int}	Young's modulus at the gluten-starch interface	kPa	Cohesion:10^6 Non-cohesion : 10^{-6}	
$\mathbf{F}$	Deformation gradient			
G_i	Shear elastic modulus of material i	Pa	$\frac{E_i}{2(1+\nu_i)}$	
$\mathbf{I}$	Second-order unit tensor			
$\mathbf{I_1}$	First invariant of the left Cauchy–Green tensor			
k	Elasticity constant of the material at the interface	N/m^3		
l	Smallest dimension of the gluten strip	m	20×10^{-6}	
L	Largest dimension of the gluten strip or height of the cylinder	m	100×10^{-6}	
$\mathbf{Q}$	Stress in the 1-element viscoelastic generalised Maxwell			
r	Horizontal direction axisymmetric			
$\mathbf{S}$	Total stress tensor			
t	Time	s		
$\mathbf{u}$	Displacement vector which components are u in the directions x or r and v in direction y or z	m		
W	Strain energy density function			
x	Horizontal direction			
y	Vertical direction			
z	Vertical direction axisymmetric			
Greek letters				
β_{gluten}	Strain energy factor of gluten		T < 50-60°C: 100 T > 70-80°C: 1000	
β_{starch}	Strain energy factor of starch		T < 50-60°C: 1000 T > 70-80°C: 100	
$\boldsymbol{\varepsilon}$	Linear or Cauchy strain tensor			
ε_H	Hencky strain		$\varepsilon_H = \ln(1+\varepsilon)$	
$\dot{\varepsilon}$	Strain rate	s^{-1}		
μ	Lamé coefficient (shear modulus)			
ν_{int}	Poisson's ratio		Cohesion: 0.4999 Non-cohesion : 0.4999999999	
ν_i	Poisson's ratio of material i		~ 0.4999	
$\boldsymbol{\sigma}$	Time-independent stress tensor	Pa		
σ	Stress	Pa		
$\boldsymbol{\tau}$	Viscoelastic stress tensor	Pa		
$\boldsymbol{\gamma}$	Infinitesimal shear strain tensor			
$\dot{\boldsymbol{\gamma}}$	Shear strain rate	s^{-1}		
λ_r	Relaxation time	s		
Super and sub -script				
el	Elastic			
eq	Equivalent			
int	Interface			
Iso	Isochoric			
n	Normal direction			
t	Tangential direction			
$\mathbf{T}$	Transpose			
vm	Von Mises			
vol	Volumetric			
∞	Infinity symbol			